

Polymer-Based Terbium Complex as a Fluorescent Probe for Cancer Antigen 125 Detection: A Promising Tool for Early Diagnosis of Ovarian Cancer

Magda M. Mohamed, Hisham Gamal, Akram El-Didamony, Ahmed O. Youssef, Esraa Elshahat, Ekram H. Mohamed, and Mohamed S. Attia*



Cite This: *ACS Omega* 2024, 9, 24916–24924



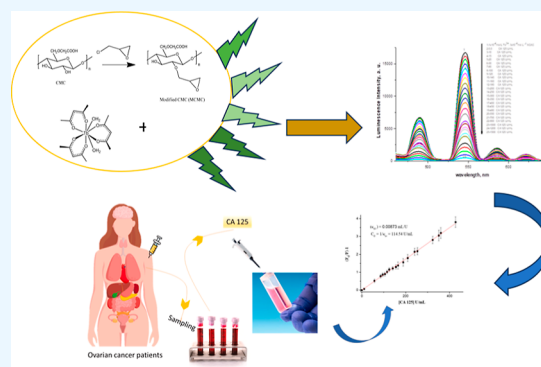
Read Online

ACCESS |

Metrics & More

Article Recommendations

ABSTRACT: A novel photoprobe, Tb–acetylacetonate (Tb–ACAC) doped within a modified epoxy cellulose polymer immobilized with CA-125 monoclonal antibody, offers an accurate and highly selective method for early ovarian cancer (OC) diagnosis by detecting cancer antigen 125 (CA-125) in serum samples. This approach leverages quenching of the Tb–ACAC luminescence upon binding to CA-125. Characterization of the photoprobe film through UV–vis and fluorescence measurements confirmed the presence of Tb–ACAC within the polymer matrix. In aqueous solution (pH 6.8, $\lambda_{\text{ex}} = 365$ nm), the characteristic emission band of Tb–ACAC at $\lambda_{\text{em}} = 546.2$ nm exhibited significant quenching upon CA-125 binding. This quenching effect enabled the sensitive and specific detection of CA-125 in diverse serum samples from OC patients, demonstrating the applicability, simplicity, and effectiveness of this novel approach.



1. INTRODUCTION

The quest for efficient sensors hinges on two crucial pillars: sensitivity and selectivity. Recognizing this, researchers have explored diverse avenues, including nanoparticles, to amplify signal response and unlock novel biosensing possibilities for biomedical applications.^{1,2} Among these, luminescent complexes, particularly lanthanide (Ln) complexes, stand out for their unique photophysical advantages.^{3–5} Their high brightness, photostability, narrow emission bands, long lifetimes, and biocompatibility, coupled with large surfaces for biomolecule attachment, make them ideal candidates for bioanalytical applications.⁵ Lanthanide complexes excel in both detection and sensing capabilities. Their narrow emission bands enable multitarget detection, while long-lived luminescence facilitates time-resolved techniques, eliminating short-lived background noise and boosting sensitivity compared to conventional sensors.^{6,7} This remarkable optical performance has fueled their widespread application in cellular and small animal imaging, where background autofluorescence is absent.^{6,7} Furthermore, lanthanide sensors boast high signal-to-noise ratios, translating to highly sensitive and selective diagnoses.⁸ The potent and specific interactions between terbium complexes and biomolecules, even *in vivo*, pave the way for exceptional detection sensitivity and selectivity.⁸ Ovarian cancer (OC) presents a formidable challenge, claiming the lives of over 152,000 women annually despite being the leading cause of death among gynecological malignancies.⁹ Early diagnosis is

paramount for improved survival rates, yet available tools fall short of ideal screening efficacy.¹⁰ While tumor markers, imaging techniques, and combined algorithms have been employed to differentiate benign from malignant epithelial OC, the search for improved sensitivity and specificity continues.^{11,12} CA-125, the most commonly used biomarker for OC detection, faces limitations.¹³ While elevated levels in advanced stages make it valuable for postsymptomatic detection, its ambiguous results in early stages have led medical societies to advise against routine screening for average-risk women.^{14,15} Despite its limitations, CA-125 remains crucial for monitoring treatment response, disease-free survival duration, and predicting prognosis.^{16–22} The standard enzyme-linked immune sorbent assay (ELISA) method, while established, has limitations.²³ The ELISA encounters three main limitations; first, the interfering compounds in the sample matrices can adversely impact the accuracy and precision of the assay. In addition, the lack of standard procedures and insufficient data interpretation and analysis could lead to high variability in ELISA's performance

Received: February 24, 2024

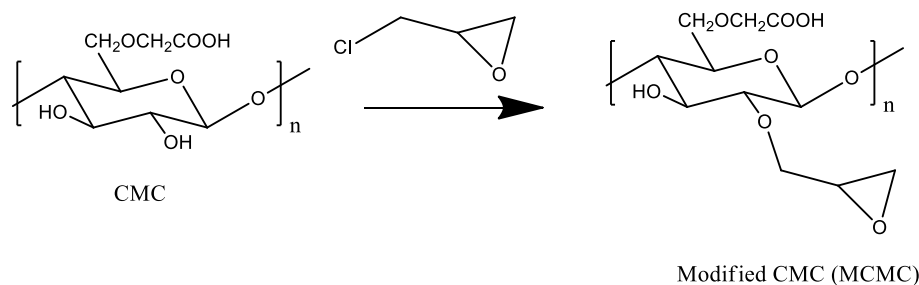
Revised: April 30, 2024

Accepted: May 21, 2024

Published: June 1, 2024



Scheme 1. Schematic Preparation of Epoxy-Functionalized CMC



including reproducibility and sensitivity. The ELISA has other restrictions such as prozone effect, analytical noise, and limits of detection and quantitation. Moreover, ELISAs are expensive and demand sophisticated and complex instruments.^{24–26} The newer techniques like Raman spectroscopy,^{27–29} mass spectrometry,^{30,31} and electrochemical impedance spectroscopy^{32,33} offer enhanced sensitivity and specificity, but their complexity, cost, and operational demands hinder wider clinical application.^{34–36} On the other hand, a spectrofluorimetric technique in general offers some merits including simplicity, sensitivity, and reliability due to its superior analytical performance.³⁷ Thus, a spectrofluorimetric technique provides both cost-effective and easy-to-implement analytical methods that could be amended to be used in different clinical applications providing accurate results.^{38,39} Coupling spectrofluorimetric techniques with nanotechnology offers a powerful approach for various applications.^{40,41} Furthermore, coupling nanotechnology and smart nanomaterials with spectrofluorimetric methods allowed the fabrication of different optical sensors that permitted the direct probing of trace analytes and diagnostic biomarkers. The nano-optical biosensors enhanced the sensitivity of spectrofluorimetric methods via reducing detection and quantitation limits and improving trace analysis even in small sample sizes. The integration of nanotechnology with spectrofluorimetric techniques opens avenues for enhanced therapeutics, diagnostics, and nanoparticle characterizations.^{42–45} This work presents a novel approach: a thin film terbium complex doped in modified epoxy cellulose polymer, immobilized with a CA-125 monoclonal antibody. This sensor assesses CA-125 as a biomarker for early OC diagnosis by measuring the quenching of its fluorescence intensity at 546.2 nm upon excitation at 365 nm in water. This innovative method holds immense potential for overcoming the limitations of current techniques and paving the way for more accurate and efficient early detection of OC.

2. EXPERIMENTAL SECTION

2.1. Materials. $\text{Tb}(\text{NO}_3)_3 \cdot 5\text{H}_2\text{O}$ (purity, 99.0%) and acetylacetone (ACAC) were purchased from Sigma-Aldrich (Saint Louis, USA). Ethyl acetate, NaH_2PO_4 , and NaOH were purchased from Sigma-Aldrich. NaCl, KCl, albumin, uric acid, urea, triglyceride, and glucose were purchased from Sigma. Monoclonal antibody of CA 125 and cancer antigen 125 (CA-125) (0.1 mg) were purchased from orb98857, Biorbyt. Human blood samples were collected from the New Al-Kasr-EL-Aini Teaching Hospital Cairo University and Ain Shams Specialized Hospital, Ain Shams University, Cairo, Egypt, between February 2022 and April 2023 in accordance with the World Health Organization (WHO)-approved protocol for human specimen collection and for the use of this material and related clinical information for research purposes.

2.2. Reagents and Solutions. The working solutions of CA-125 and monoclonal antibody of CA 125 were prepared by dissolving 0.1 mg of the biomarker and antibody in water. The phosphate buffer of pH 7.2 was prepared by mixing 100 mL of 0.1 mol L⁻¹ NaH_2PO_4 with 58.2 mL of 0.1 mol L⁻¹ NaOH and volume is completed to 200 mL by distilled water.

2.3. Instrumentation. All fluorescence measurements were recorded with a Meslo-PN (222-263000) Thermo Scientific Lumina fluorescence spectrometer in the range of 190–900 nm available at Ain Shams University, Cairo, Egypt. The absorption spectra were recorded with a Thermo UV–visible double-beam spectrophotometer. All pH measurements were made with a pHs-Janway 3040 ion analyzer.

2.4. Sample Preparation. After a standard history and physical examination, blood was drawn for routine laboratory measures. Serum samples were collected from all the volunteers; (i) control subjects (10 samples), (ii) patients' OC (15 samples). A 3.0 mL portion of citrate solution was added to 4.0 mL of plasma, and the solution was centrifuged for 15.0 min at 4000 rpm to remove all proteins. After decantation, 1.0 mL of the serum was added with 0.1 mL of the buffer (pH = 7.2) to the thin film of the nano-optical sensor in the cuvette, and finally, 1.9 mL of water was added to give the test solution.

2.5. Proposed Method. The performance of a novel biosensor for cancer antigen 125 (CA-125) detection was evaluated by using a terbium ACAC (Tb–ACAC) complex doped in a modified epoxy cellulose polymer. Standard CA-125 solutions (100 μL) at various concentrations were incubated with the thin film sensor followed by fluorescence measurement at 365 nm excitation and 546.2 nm emission. After each measurement, the sensor was rinsed with water. A calibration plot was constructed by plotting the normalized fluorescence intensity ($F_0/F - 1$) at 546.2 nm against the CA-125 concentration. For serum sample analysis, 100 μL aliquots were diluted to 3 mL in the presence of the sensor, and fluorescence intensity was measured at 546.2 nm.

2.5.1. Performance Metrics. The sensitivity, specificity, positive predictive value (PPV), and negative predictive value (NPV) were calculated by using the following formulas.

- Sensitivity: $A/(A + B) \times 100\%$ (where A is the number of true positives and B is the number of false negatives)
- Specificity: $C/(C + D) \times 100\%$ (where C is the number of true negatives and D is the number of false positives)
- PPV: $A/(A + D) \times 100\%$
- NPV: $C/(C + B) \times 100\%$

Prevalence: $T_{\text{disease}}/\text{total} \times 100\%$ (where T_{disease} is the number of individuals with the disease and total is the total number of individuals tested)

2.5.2. Preparation of Modified Polysaccharide. 3 g of carboxymethyl cellulose (CMC) was dissolved (suspended) in

100 mL of water followed by the addition of 4 mL of epichlorohydrin. The activation process was conducted at 65 °C for 3 h using a water bath. To promote the reaction of epichlorohydrin with hydroxyl groups of CMC, the pH of the reaction mixture was maintained basic by addition of a dilute NaOH solution. After that, the solution was allowed to cool, and the solution was cast in a Petri dish and allowed to dry at 25 °C overnight.

Preparation of the Epoxy-Functionalized CMC Thin Film-Embedded Tb–ACAC Complex

After preparation of the epoxy-functionalized CMC in Scheme 1, 10 mL of the prepared epoxy-functionalized CMC was mixed with 5 mL of Tb–ACAC complex for about 5 min. Then a thin film is obtained by using a spin coater at 500 rpm.

3. RESULTS AND DISCUSSION

3.1. SEM Characterization. The SEM image of the pure epoxy cellulose polymer is shown in Figure 1A. The surface

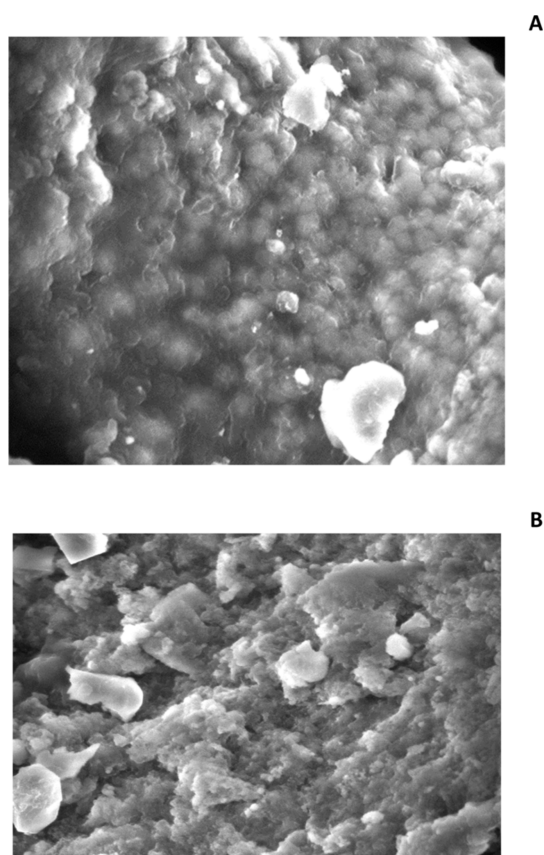


Figure 1. SEM image of epoxy cellulose polymer (a) and the epoxy cellulose polymer-embedded Tb–ACAC complex (b).

appears relatively uniform with a granular texture typical for this kind of polymer composite. This morphology can be attributed to the cellulose fibers or particles embedded within the epoxy matrix, giving rise to a rough surface texture. After embedding of the Tb–ACAC complex in the epoxy cellulose polymer (Figure 1B), the SEM image displays the presence of the Tb–ACAC complex, which seems to alter the surface morphology. The embeddings of the complex are evidenced by the distinct, brighter areas that contrast with the darker background of the cellulose epoxy matrix. The change in contrast could reflect the difference in electron density and atomic number between the

terbium complex and the surrounding polymer matrix, as elements with a higher atomic number scatter electrons more effectively.

3.2. Absorption Spectra. Figure 2 depicts the absorption spectra of ACAC and its Tb complex embedded within a

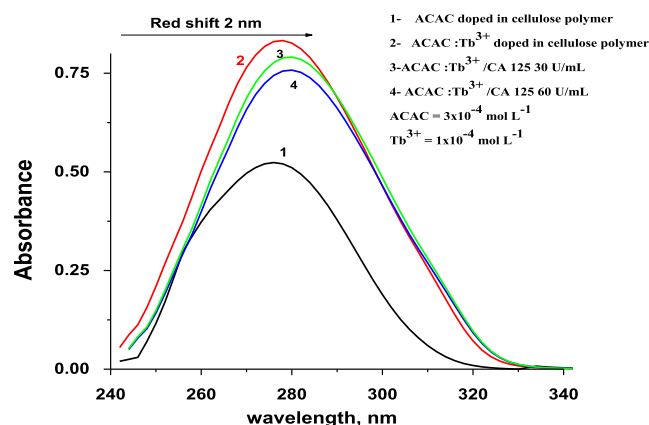


Figure 2. Absorption spectra of 3.0×10^{-4} mol L⁻¹ of ACAC doped in cellulose polymer (1), Tb³⁺–ACAC complex in a ratio of 1.0×10^{-4} / 3.0×10^{-4} mol L⁻¹ doped in cellulose polymer (2), Tb³⁺–ACAC complex/CA 125 (30 U/mL) doped in cellulose polymer (3), and Tb³⁺–ACAC complex/CA 125 (60 U/mL) doped in cellulose polymer (4), all measured at pH 6.8.

cellulose polymer matrix, revealing its light absorption characteristics across various wavelengths. The dominant peak at 276 nm in the ACAC spectrum arises from an n– π transition within the carbonyl group, while the Tb-complex spectrum exhibits a peak at 278 nm attributed to a π – π transition in its aromatic ring. Notably, the presence of increasing CA 125 concentrations instigates a red shift of the Tb-complex peak from 278 to 280 nm, accompanied by a concomitant decrease in peak intensity. This phenomenon can be ascribed to the formation of a Tb–ACAC–CA 125 complex, where the bound CA 125 quenches the aromatic ring's π – π^* transition, leading to the observed intensity reduction. Importantly, this spectral response paves the way for the development of a highly sensitive CA 125 sensor. The envisioned sensor would leverage the observed changes in the Tb-complex absorption spectrum upon CA 125 binding, enabling the detection of this crucial biomarker in biological samples like blood.

3.3. Emission Spectra. The emission spectra of Tb³⁺ luminescence in varying ACAC concentrations doped in cellulose polymer are presented in Figure 3. Curve 1 reveals minimal emission for the isolated Tb³⁺ ions. Adding ACAC to the Tb³⁺ solution introduces characteristic Tb³⁺ peaks at ⁵D₄ transitions to ⁷F₆, ⁷F₅, and ⁷F₄ (compare curves 2 and 1). Notably, curve 4 compared to curves 2 and 3 in Figure 3 shows an enhanced peak at $\lambda_{em} = 546.2$ nm upon ACAC addition, suggesting efficient energy transfer from ACAC to Tb³⁺ within the complex.

3.4. Effect of Experimental Variables. **3.4.1. Effect of pH.** Figure 4 presents the emission spectra of the Tb³⁺–ACAC complex embedded within the cellulose polymer at varying pH values (2.85–10.4). The characteristic green luminescence peak of Tb³⁺ at 546.2 nm exhibits a pronounced pH dependence, reaching its maximum intensity at pH 6.8. This behavior can be attributed to several key factors: protonation of ACAC ligands: at acidic pH (2.85 and 4), ACAC ligands become protonated

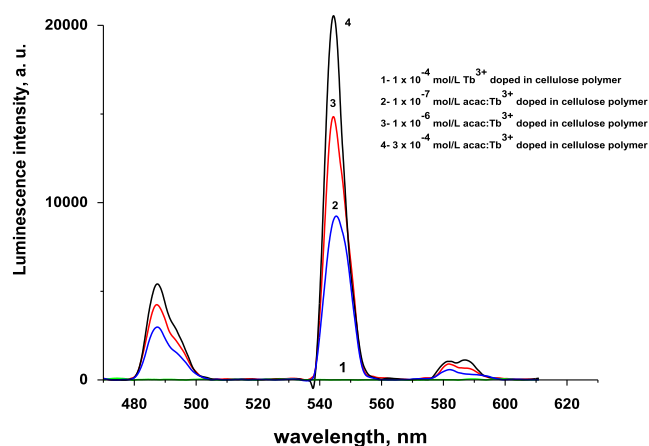


Figure 3. Luminescence emission spectra of $1.0 \times 10^{-4} \text{ mol L}^{-1} \text{ Tb}^{3+}$ in different concentrations of ACAC; (1) $1.0 \times 10^{-4} \text{ mol L}^{-1}$ ACAC, (2) $1.0 \times 10^{-7} \text{ mol L}^{-1}$ ACAC, (3) $1.0 \times 10^{-8} \text{ mol L}^{-1}$ ACAC, and (4) $3.0 \times 10^{-4} \text{ mol L}^{-1}$ ACAC doped in cellulose polymer at pH 6.8 and $\lambda_{\text{em}} = 546.2 \text{ nm}$.

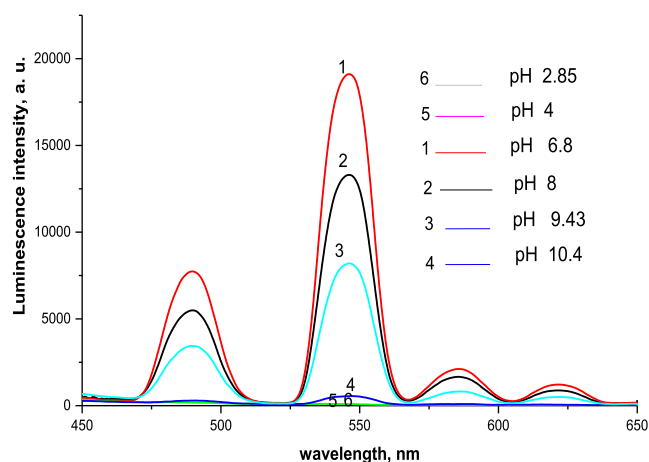


Figure 4. Luminescence emission spectra of Tb^{3+} -ACAC in ratio $1.0 \times 10^{-4} / 3.0 \times 10^{-4} \text{ mol L}^{-1}$ doped in cellulose polymer at different pHs (1) 6.8, (2) 8, (3) 9.43, (4) 10.4, (5) 4, and (6) 2.85 and $\lambda_{\text{ex}} = 365 \text{ nm}$ in water.

(HAcac), hindering efficient light absorption and energy transfer to Tb^{3+} due to altered electronic structures and excited-state properties. This explains the diminished luminescence intensity at these pH values. Complex hydrolysis: basic pH (9.43 and 10.4) might induce hydrolysis of the Tb^{3+} -ACAC complex, where water molecules partially replace ACAC ligands, forming Tb^{3+} -hydroxide species with distinct luminescence characteristics compared with the intact complex. This could contribute to the slight intensity decrease observed at these pH values. Formation of Tb^{3+} -hydroxide species: as mentioned above, Tb^{3+} -hydroxide species formed at higher pH generally exhibit weaker luminescence due to quenching mechanisms involving OH^- groups, further contributing to the observed intensity decreases at pH 9.43 and 10.4. Optimal ligand configuration: at pH 6.8, deprotonated ACAC ligands (Ac^-) might adopt a specific configuration around Tb^{3+} that optimizes energy transfer from the ligand to the metal ion, leading to the observed maximum luminescence intensity at this particular pH value. In summary, the pH-dependent luminescence behavior of the Tb^{3+} -ACAC complex likely arises from an interplay among protonation-induced changes in ligand properties, complex

hydrolysis at high pH, formation of Tb^{3+} -hydroxide species, and an optimal ligand configuration for energy transfer at pH 6.8.

3.4.2. Emission Spectra. Figure 5 showcases the emission spectra of the Tb^{3+} -ACAC complex, unveiling a compelling

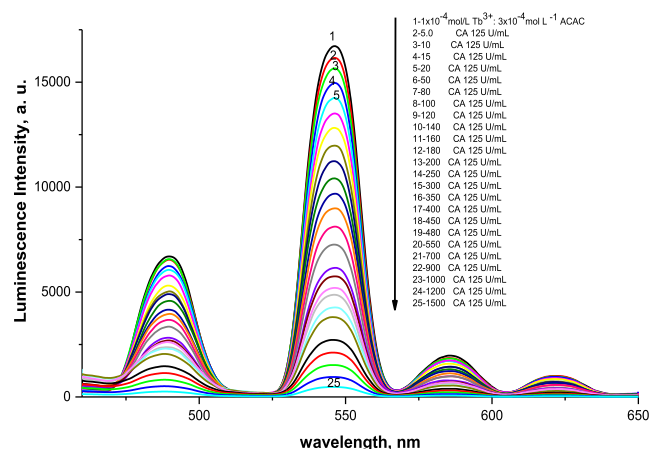


Figure 5. Luminescence emission spectra of the Tb^{3+} -ACAC complex in ratio $1.0 \times 10^{-4} / 3.0 \times 10^{-4} \text{ mol L}^{-1}$ doped in cellulose polymer in the presence of different concentrations of CA 125 ranging from 5 to 1500 U/mL in water at $\lambda_{\text{ex}} = 365 \text{ nm}$ and pH 6.8.

narrative as CA-125 concentration ascends from 5 to 1500 U/mL. The protagonist, the characteristic green luminescence of Tb^{3+} at 546.2 nm, experiences a dramatic dimming with increasing CA-125, solidifying the protein's quenching prowess. Supporting actors, weaker emission bands corresponding to Tb^{3+} transitions, echo this quenching, albeit less vehemently. Remarkably, even the lowest CA-125 concentration (5 U/mL) elicits a subtle dimming, hinting at the exceptional sensitivity of the Tb^{3+} -ACAC complex toward its binding partner. Several potential culprits lurk behind this CA-125-induced luminescence quenching, each wielding a distinct modus operandi: Förster resonance energy transfer (FRET): when CA-125 binds intimately with the Tb^{3+} -ACAC complex (within the Förster distance, typically $<10 \text{ \AA}$), it can act as a stealthy energy thief, siphoning energy from the excited Tb^{3+} and reducing its luminescence. The observed quenching at low CA-125 concentrations suggests a possible spectral alignment between the Tb^{3+} -ACAC emission and CA-125 absorption, facilitating efficient FRET. Static quenching: in this scenario, CA-125 directly interacts with the excited Tb^{3+} -ACAC complex, disrupting its electronic structure and energy levels. This introduces alternative nonradiative decay pathways, diminishing the luminescence intensity without any energy transfer. Microenvironmental shifts: CA-125 binding might alter the local environment surrounding the Tb^{3+} ion, affecting solvent accessibility and influencing excited-state dynamics, even without direct energy transfer or excited-state perturbation. This captivating interplay between CA-125 and Tb^{3+} -ACAC luminescence paves the way for the development of promising biosensing platforms for early OC detection. The exceptional sensitivity observed in this study holds immense potential for detecting CA-125 at clinically relevant concentrations. However, the journey continues: (1) optimizing sensitivity and specificity: exploring different Tb^{3+} complexes, modifying the ACAC ligand, or incorporating signal amplification strategies could further enhance the detection prowess. (2) Bridging the

gap to practical diagnostics: translating this into a user-friendly assay format suitable for clinical settings is crucial for real-world implementation. (3) Unveiling the dominant quenching mechanism: elucidating the primary culprit behind the quenching effect will guide further optimization and design of even more potent biosensing probes.

3.5. Analytical Performance. 3.5.1. Method Validation.

3.5.1.1. Dynamic Range. The present study delves into the fascinating realm of early OC detection, utilizing a meticulously crafted terbium (Tb^{3+}) complex-doped epoxy cellulose polymer biosensor. This innovative approach leverages the interaction between the sensor and cancer antigen 125 (CA-125), a crucial biomarker for the disease. Our investigation unveils the intricate quenching mechanism responsible for the sensor's response, paving the way for further optimization and clinical translation. A hallmark of our findings lies in the linear relationship between the fluorescence intensity quenching and CA-125 concentration, as depicted in Figure 6.⁴⁶ This linearity beautifully

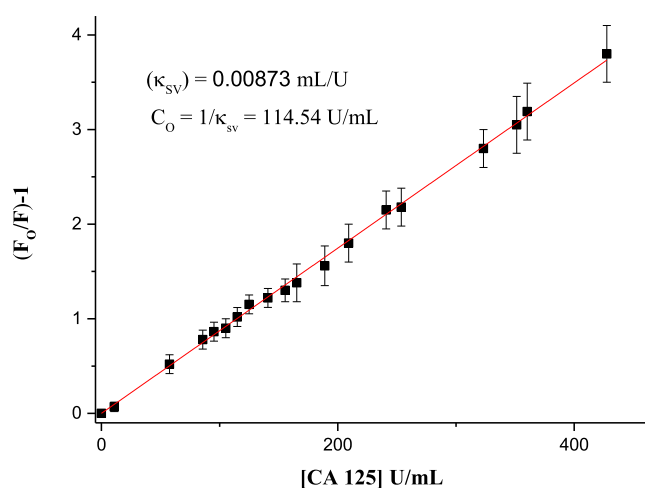


Figure 6. Linear relationship between $[(F_0/F) - 1]$ and the corresponding [CA 125] concentrations at pH 6.8. Slope = Stern–Völmer constant = κ_{sv} ; half-quenching concentration ($C_{1/2}$) = $1/\kappa_{sv}$; Förster distance (R_0) at a mere $1.51 \text{ \AA} = 7.35 \times \sqrt[3]{1/C_{1/2}}$.

corroborates the applicability of the Stern–Völmer equation, which is a cornerstone in understanding luminescence quenching phenomena. By delving deeper, we calculated the Stern–Völmer constant (κ_{sv}) to be $0.0087 \text{ mol}^{-1} \text{ L}$, indicating a moderate sensitivity toward CA-125. This value, coupled with the half-quenching concentration ($C_{1/2}$) of 114.7 U mL^{-1} , allowed us to estimate the Förster distance (R_0) at a mere 1.51 \AA . Remarkably, this value falls significantly short of the typical FRET range ($10\text{--}100 \text{ \AA}$), strongly suggesting static quenching as the dominant mechanism at play. This implies that CA-125 molecules directly bind to the Tb^{3+} complex, perturbing its excited state and fostering nonradiative decay pathways, ultimately leading to a reduction in luminescence intensity. The observed linearity further bolsters the static quenching hypothesis. However, a potential FRET contribution at higher quencher concentrations cannot be entirely ruled out. The nonzero intercept in the Stern–Volmer plot hints at this possibility, warranting further exploration through techniques like time-resolved luminescence measurements to definitively quantify the contributions of each mechanism. While the sensor exhibits moderate sensitivity, it holds immense promise for further improvement. Exploring various Tb^{3+} complexes,

tailoring the cellulose matrix, and incorporating signal amplification strategies are potential avenues to enhance sensitivity in future iterations. Notably, our data analysis assumes a single binding site model for CA-125 on the Tb^{3+} complex. If multiple binding sites are present, then the quenching behavior could become more intricate, necessitating a more comprehensive analysis. Beyond the quenching mechanism, our sensor boasts additional strengths. The fluorescence intensity at 546.2 nm exhibits a remarkable linear decrease with CA-125 concentrations ranging from 0.5 to 478 U mL^{-1} , with an impressive correlation coefficient of 0.999 . This wide linear range signifies the sensor's versatility across a clinically relevant spectrum. Furthermore, the calculated detection limit (LOD) of 0.09 U mL^{-1} underscores the sensor's remarkable sensitivity, surpassing many existing methods, Table 1.⁴⁷ A comparative analysis with previously published

Table 1. Sensitivity and Regression Parameters for the Proposed Method^a

parameter	value
$\lambda_{ex}/\lambda_{em}$ (nm)	365/546.2
linear range (U/mL)	0.5–478
LOD (U/mL)	0.09
limit of quantification (U/mL)	0.27
regression equation, Y^*	$Y = a + bX$
intercept (a)	0.001
slope (b)	0.0087
standard deviation	0.01
variance (Sa^2)	1.0×10^{-4}
regression coefficient (r)	0.999

^aWhere Y = fluorescence intensity, X = concentration in U/mL, a = intercept, and b = slope.

techniques showcases the superiority of our sensor. It demonstrates exceptional stability, a significantly lower LOD, and a broader linear range, solidifying its potential for clinical applications.^{48–72} In conclusion, this study offers a multifaceted exploration of the terbium complex-doped epoxy cellulose polymer sensor's interaction with CA-125. The unveiled quenching mechanism, dominated by static quenching with a possible FRET component, lays the groundwork for future optimization. The sensor's impressive sensitivity, wide linear range, and low LOD position it as a promising candidate for early OC detection, paving the way for more effective patient management and improved clinical outcomes.

3.5.1.2. Selectivity. Figure 7 shows the effect of various interfering species on the fluorescence intensity of a Tb –ACAC complex-doped sensor film upon addition of CA-125. The sensor's response to CA-125 is monitored by measuring the quenching of the Tb^{3+} emission peak at 546.2 nm . Tumor markers: carcinoembryonic antigen, carbohydrate antigen 19-9 (CA 19-9), and carbohydrate antigen 15-3 (CA 15-3). Electrolytes: sodium chloride (NaCl) and potassium chloride (KCl). Biomolecules: albumin, uric acid, urea, triglyceride, and glucose. Each bar in the figure represents the relative change in fluorescence intensity (expressed as a percentage) compared to that of the control (sensor with CA-125 only) after adding the respective interfering species. A decrease in fluorescence intensity indicates quenching of the Tb^{3+} luminescence, potentially due to interaction of the interfering species with the sensor or competition with CA-125 for binding sites. Most interfering species show a minimal to negligible effect on the

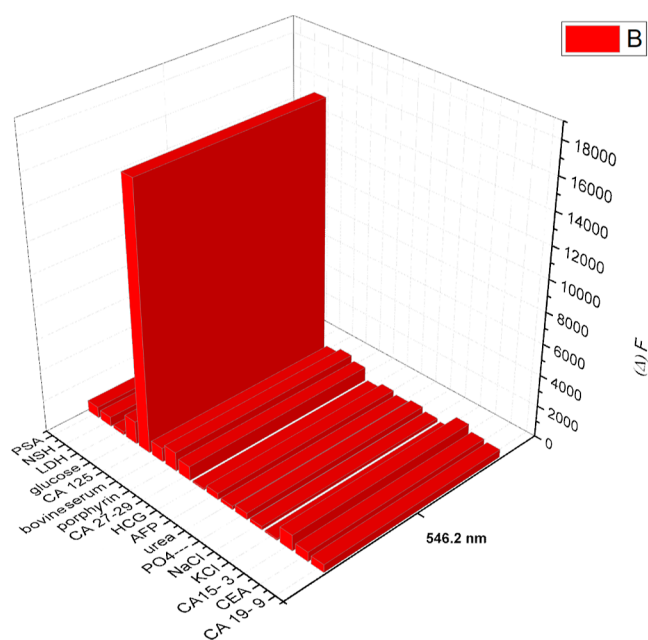


Figure 7. Effect of the interfering species on the fluorescence intensity of the optical sensor.

sensor's response to CA-125, with fluorescence changes within the tolerable limit of $\pm 3\%$. This suggests high selectivity of the sensor toward CA-125. Among the tumor markers, only CA 19-9 exhibits a slightly higher quenching effect (around -5%), indicating potential cross-reactivity to some extent. However, the difference compared with the control remains relatively small. Electrolytes (NaCl and KCl) and biomolecules like albumin, uric acid, and urea have negligible impact, further confirming the sensor's resistance to common biological components. Interestingly, total protein and triglyceride show

a slight enhancing effect on the sensor's response to CA-125, with fluorescence increases of around 2–3%. This could be due to complex interactions with the sensor matrix that might facilitate CA-125 binding or enhance the luminescence efficiency of the Tb^{3+} complex. The data demonstrate the promising selectivity and anti-interference ability of the Tb–ACAC complex-doped sensor for CA-125 detection. While slight cross-reactivity with CA 19-9 and potential matrix effects with total protein and triglyceride warrant further investigation, the sensor shows significant potential for practical applications in biological sample analysis.

3.5.1.3. Accuracy and Precision of the Method. The data in Table 2 shows the average intraday and interday accuracy and precision of the proposed method for the determination of CA 125 by the thin film-doped nano-Tb–ACAC complex doped in modified epoxy cellulose polymer, compared to a standard method. Table 2 shows that the proposed method has higher accuracy (accuracy was expressed as percentage recovery and percentage RSD) and precision than the standard method for both intraday and interday analysis. The intraday accuracy of the proposed method is 102.60%, with a relative error (RE) of 2.60% and a recovery percentage of 102.60%. The interday accuracy of the proposed method is 106.7%, with an RE of 6.7% and a recovery percentage of 106.7%. The standard method has an intraday accuracy of 97.33%, with an RE of -2.6% and a recovery percentage of 97.33%. The interday accuracy of the standard method is 101.2%, with an RE of 1.2% and a recovery percentage of 101.2%. The confidence limit (CL) values show the variability of the data. The CL values for the proposed method are smaller than the CL values for the standard method, indicating that the proposed method is more precise. The RSD % values show the relative standard deviation of the data. The RSD % values for the proposed method are also smaller than the RSD % values for the standard method, indicating that the proposed method is more reproducible. Overall, the data in

Table 2. Evaluation of Intraday and Interday Accuracy and Precision^a

sample	standard method average U/mL	proposed method											
		intraday accuracy and precision ($n = 3$)						interday accuracy and precision ($n = 3$)					
		average found U/mL	$\pm CL$	RE %	t -test	102.60	1.92	average found U/mL	$\pm CL$	RE %	t -test	recovery %	RSD %
1	16.5	16.93	0.54	2.60	0.47	102.60	1.92	17.60	0.58	6.7	0.29	106.7	2.08
2	33	32.12	0.82	-2.6	0.96	97.333	1.31	33.40	0.88	1.2	0.10	101.2	1.43
3	24.75	25.35	1.04	2.42	0.65	102.42	1.49	26.36	1.11	6.5	0.43	106.5	1.62
4	26.4	27.05	0.78	2.46	0.71	102.46	1.78	28.13	0.83	6.5	0.46	106.5	1.93
5	29.7	30.7	1.51	3.36	1.09	103.36	3.34	31.92	1.61	7.5	0.60	107.5	3.63
6	254.1	257.42	2.37	1.30	3.64	101.30	1.28	267.7	2.53	5.3	3.67	105.3	1.40
7	323.4	321.42	3.94	-0.6	2.17	99.387	1.69	334.2	4.21	3.3	2.91	103.3	1.84
8	396	401.61	2.74	1.41	6.16	101.41	0.94	417.6	2.92	5.4	5.83	105.4	1.02
9	277.2	278.21	2.77	0.36	1.10	100.36	1.39	289.3	2.96	4.3	3.27	104.3	1.51
10	359.7	354.68	2.44	-1.3	5.50	98.604	0.93	368.8	2.61	2.5	2.45	102.5	1.01
11	372.9	375.21	5.28	0.61	2.53	100.61	1.94	390.2	5.64	4.6	4.67	104.6	2.11
12	343.2	340.51	6.90	-0.7	2.95	99.216	2.76	354.1	7.38	3.1	2.94	103.1	3.002
13	653.4	656.7	6.45	0.50	3.62	100.50	2.45	682.9	6.90	4.5	7.97	104.5	2.675
14	623.7	627	3.47	0.52	3.62	100.52	2.87	652.0	3.71	4.5	7.64	104.5	3.12
15	759	772.2	4.78	1.73	14.50	101.73	1.94	803.0	5.11	5.8	11.89	105.8	2.11

^a% RE, percent relative error. % RE = $[(\text{concentration proposed} - \text{concentration known}) / \text{concentration known}] \times 100$, % RSD, relative standard deviation. % RSD = $[S / (\text{average measurements})] / 100$, and $\pm CL$, confidence limits: $CL = tS / n^{(1/2)}$. The tabulated value of t is 4.303, at a 95% confidence level; S = standard deviation and n = number of measurements; % recovery = $\bar{A}_{(\text{PROPOSED METHOD})} / \bar{A}_{(\text{STANDARD METHOD})} \times 100$; \bar{A} = average concentration value = $(X_1 + X_2 + X_3) / 3$.

Table 2 show that the proposed method is a more accurate, precise, and reproducible method for the determination of CA 125 than the standard method. This suggests that the proposed method has the potential to be a valuable analytical tool for the clinical determination of CA 125.

3.5.1.4. Application. Analytical utility: Table 2 compares the proposed method with the standard method for measuring CA-125 concentration in two groups: healthy patients and OC patients. Average values: both methods show similar average values for both groups. For healthy patients, the proposed method yields slightly higher values (12.10–29.50 U mL⁻¹) compared to the standard method (12.0–29.0 U mL⁻¹). Similarly, for OC patients, the proposed method gives slightly higher values (77.40–234.0 U mL⁻¹) compared to the standard method (77.0–230.0 U mL⁻¹). Standard deviations: both methods also exhibit similar standard deviations within each group, suggesting comparable variability in measurements. Statistical significance: there are no significant differences between the two methods, which suggests a high degree of agreement between their results.

Diagnostic performance: the diagnostic performance of the proposed method is represented by the following results: sensitivity: 97.35%—this indicates a high probability of correctly identifying patients with OC. Specificity: 94.29%—this indicates a high probability of correctly identifying patients without OC. PPV: 89.45%—this indicates that when the test result is positive, there is an 89.45% chance that the patient truly has OC. NPV: 91.75%—this indicates that when the test result is negative, there is a 91.75% chance that the patient does not have OC. Prevalence of disease: 71.51%—this indicates the proportion of patients in the tested population who have OC.

4. CONCLUSIONS

The proposed method has a wider linear dynamic range and lower LOD than the standard method for both intraday and interday measurements. The proposed method also has a higher average recovery % and lower RSD % than the standard method for both intraday and interday measurements. These results indicate that the proposed method is more accurate and precise than the standard method. Specifically, the proposed method has a linear dynamic range of 0.5–478 U/mL for intraday measurements and 16.93–334.2 U/mL for interday measurements. The standard method has a linear dynamic range of 16.5–254.1 U/mL for intraday measurements and 17.60–267.7 U/mL for interday measurements. The proposed method has a LOD of 0.09 U/mL, while the standard method has a LOD of 2.32 U/mL. The proposed method has an average recovery % of 102.46% for intraday measurements and 103.30% for interday measurements. The standard method has an average recovery % of 101.30% for intraday measurements and 101.20% for interday measurements. The proposed method has an RSD % of 1.92% for intraday measurements and 1.84% for interday measurements. The standard method has an RSD % of 2.60% for intraday measurements and 2.53% for interday measurements.

AUTHOR INFORMATION

Corresponding Author

Mohamed S. Attia – Chemistry Department, Faculty of Science, Ain Shams University, Cairo 11566, Egypt; orcid.org/0000-0001-6074-7366; Email: Mohamed_Sam@yahoo.com

Authors

Magda M. Mohamed – Chemistry Department, Faculty of Science, Ain Shams University, Cairo 11566, Egypt
Hisham Gamal – Aeromedical Council Laboratories-Ministry of Civil Aviation, Cairo 3753450, Egypt
Akram El-Didamony – Chemistry Department, Faculty of Science, Zagazig University, Zagazig 44519, Egypt
Ahmed O. Youssef – Chemistry Department, Faculty of Science, Ain Shams University, Cairo 11566, Egypt
Esraa Elshahat – Clinical Pathology Department, Faculty of Medicine, Ain Sham University, Cairo 11566, Egypt
Ekram H. Mohamed – Pharmaceutical Chemistry Department, Faculty of Pharmacy, The British University in Egypt, El-Sherouk 11837, Egypt

Complete contact information is available at:

<https://pubs.acs.org/10.1021/acsomega.4c01814>

Notes

The authors declare no competing financial interest.

ACKNOWLEDGMENTS

I would like to express my sincere gratitude to Professor Mohamed S. Mohy-Eldin “Polymer Materials Research Department, Advanced Technology and New Materials Research Institute” for his invaluable contribution to this study. Professor Mohy-Eldin provided critical support by performing Raman and DSC spectroscopic measurements of the polymer sample.

REFERENCES

- (1) Ahmed, Sh.; Shaikh, N.; Pathak, N.; Sonawane, A.; Pandey, V.; Maratkar, S. An overview of sensitivity and selectivity of biosensors for environmental applications. In *Tools, Techniques and Protocols for Monitoring Environmental Contaminants*, Elsevier, 2019. DOI: 10.1016/B978-0-12-814679-8.00003-0.
- (2) Ramesh, M.; Janani, R.; Deepa, C.; Rajeshkumar, L. Nano-technology-Enabled Biosensors: A Review of Fundamentals, Design Principles, Materials, and Applications. *Biosensors* **2022**, *13*, 40.
- (3) Goetz, J.; Nonat, A.; Diallo, A.; Sy, M.; Sera, I.; Lecointre, A.; Lefevre, C.; Chan, C. F.; Wong, K.; Charbonnière, L. J. Ultrabright Lanthanide Nanoparticles. *ChemPlusChem* **2016**, *81*, 479.
- (4) Zhang, N.; Tang, S.-H.; Liu, Y. Luminescence behavior of a water soluble calix[4]arene derivative complex with terbium ion(III) in gelation solution. *Spectrochim. Acta, Part A* **2003**, *59* (5), 1107–1112.
- (5) Escudero, A.; Becerro, A. I.; Carrillo-Carrión, C.; Núñez, N. O.; Zyuzin, M. V.; Laguna, M.; González-Mancebo, D.; Ocaña, M.; Parak, W. J. Rare earth based nanostructured materials: synthesis, functionalization, properties and bioimaging and biosensing applications. *Nanophotonics* **2017**, *6* (5), 881–921.
- (6) Weibel, N.; Charbonniere, L. J.; Guardigli, M.; Roda, A.; Ziesler, R. Engineering of highly luminescent lanthanide tags suitable for protein labeling and time-resolved luminescence imaging. *J. Am. Chem. Soc.* **2004**, *126*, 4888–4896.
- (7) Hanaoka, K.; Kikuchi, K.; Kobayashi, S.; Nagano, T. Time-resolved long-lived luminescence imaging method employing luminescent lanthanide probes with a new microscopy system. *J. Am. Chem. Soc.* **2007**, *129*, 13502–13509.
- (8) Lee, S. Y.; Lin, M.; Lee, A.; Park, Y. I. Lanthanide-Doped Nanoparticles for Diagnostic Sensing. *Nanomaterials* **2017**, *7*, 411.
- (9) La Vecchia, C. Epidemiology of ovarian cancer: a summary review. *Eur. J. Cancer Prev.* **2001**, *10* (2), 125–129.
- (10) Warnakulasuriya, S.; Kerr, A. R. Oral Cancer Screening: Past, Present, and Future. *J. Dent. Res.* **2021**, *100* (12), 1313–1320.
- (11) Lee, Y.; Kim, Y.; Kang, J.; Nam, S.; Kim, D.; Kim, Y. Comparison of Risk of Ovarian Malignancy Algorithm and cancer antigen 125 to discriminate between benign ovarian tumor and early-stage ovarian

- cancer according to imaging tumor subtypes. *Oncol. Lett.* **2020**, *20* (1), 931–938.
- (12) Atallah, G. A.; Abd Aziz, N. H.; Teik, C. K.; Shafiee, M. N.; Kampan, N. C. New Predictive Biomarkers for Ovarian Cancer. *Diagnostics* **2021**, *11* (3), 465.
- (13) Zhang, R.; Siu, M. K. Y.; Ngan, H. Y. S.; Chan, K. K. L. Molecular Biomarkers for the Early Detection of Ovarian Cancer. *Int. J. Mol. Sci.* **2022**, *23*, 12041.
- (14) Rodríguez-Ayala, G.; Romaguera, J.; Lopez, M.; Ortiz, A. Ovarian Cancer Screening Practices of Obstetricians and Gynecologists in Puerto Rico. *BioMed Res. Int.* **2014**, *2014* (1), 920915.
- (15) Committee on Gynecologic Practice Society of Gynecologic Oncology. Committee Opinion No. 716: The Role of the Obstetrician–Gynecologist in the Early Detection of Epithelial Ovarian Cancer in Women at Average Risk. *Obstet. Gynecol.*, **2017**, *130* (3), e146 (Replaces Committee Opinion No. 477, March 2011. Reaffirmed 2019).
- (16) Thurston, D. E.; Pysz, I. *Chemistry and Pharmacology of Anticancer Drugs*, 2nd ed.; CRC Press: Boca Raton, 2021.
- (17) Charkhchi, P.; Cybulski, C.; Gronwald, J.; Wong, F. O.; Narod, S. A.; Akbari, M. R. CA125 and Ovarian Cancer: A Comprehensive Review. *Cancers* **2020**, *12* (12), 3730.
- (18) Dasgupta, A.; Wahed, A. *Tumor Markers: Clinical Chemistry, Immunology and Laboratory Quality Control*, 2nd ed.; Elsevier, 2021.
- (19) Das, C.; Mukhopadhyay, M.; Ghosh, T.; Saha, A. K.; Sengupta, M. Correlation of Cytohistological Expression and Serum Level of Ca125 in Ovarian Neoplasm. *J. Clin. Diagn. Res.* **2014**, *8* (3), 41–43.
- (20) Bast, R. C. CA 125 and the detection of recurrent ovarian cancer. *Cancer* **2010**, *116*, 2850–2853.
- (21) Santillan, A.; Garg, R.; Zahurak, M.; Gardner, G.; Giuntoli, R.; Armstrong, D.; Bristow, R. Risk of Epithelial Ovarian Cancer Recurrence in Patients With Rising Serum CA-125 Levels Within the Normal Range. *J. Clin. Oncol.* **2005**, *23*, 9338–9343.
- (22) Mohamed, Z.; Begum, S. A.; Mahmud, T.; Amatullah, M.; Khanom, A. Correlation of Preoperative Level of Serum Ca125 with Surgical Staging of Ovarian Cancer: Serum CA125 level in ovarian cancer staging. *Med. Res. Counc., Bull.* **2022**, *47*, 110–117.
- (23) Shojaeian, S.; Allameh, A.; Zarnani, A.; Chamankhah, M.; Ghods, R.; Bayat, A. A.; Jeddi-Tehrani, M. Production and Characterization of Monoclonal Antibodies against the Extracellular Domain of CA 125. *Immunol. Invest.* **2010**, *39*, 114–131.
- (24) Shan, H.-M.; Schwab, M. E.; Maurer, M. A. Development of a Sensitive Enzyme-Linked Immunosorbent Assay with Three Amplification Antibodies to Detect Low-Abundant Mouse Antibodies in the Mouse Central Nervous System. *J. Immunol.* **2023**, *210* (7), 1004–1010.
- (25) Borges, L.; Dermargos, A.; Hatanaka, E. Technical bioanalytical considerations for detection and quantification of cytokines in ELISA assays. *Cytokine* **2022**, *151*, 155615.
- (26) You, M.; Peng, P.; Xue, Z.; Tong, H.; He, W.; Mao, P.; Liu, Q.; Yao, C.; Xu, F. A fast and ultrasensitive ELISA based on rolling circle amplification. *Analyst* **2021**, *146*, 2871–2877.
- (27) Wendy, M. A molecular imaging approach combining Raman Spectroscopy and Mass Spectrometry to study biological samples. *Chim. Nouv.* **2020**, *38*, 133.
- (28) Rostron, P.; Safa, G.; Dina, G. Raman spectroscopy, review. *Int. J. Eng. Res.* **2016**, *6*, 50.
- (29) Ryabchykov, O.; Schie, I. W.; Popp, J.; Bocklitz, T. Errors and Mistakes to Avoid when Analyzing Raman Spectra. *Spectroscopy* **2022**, *37*, 48–50.
- (30) Smith, R. W. Mass Spectrometry. In *Encyclopedia of Forensic Sciences*, 3rd ed.; Elsevier, 2023.
- (31) Sharp, T. R., Mass Spectrometry. In *Drug Metabolism Handbook: Concepts and Applications in Cancer Research*, 2nd ed.; Wiley, 2022.
- (32) Quattrocchi, E.; Py, B.; Maradesa, A.; Meyer, Q.; Zhao, C.; Ciucci, F. Deconvolution of electrochemical impedance spectroscopy data using the deep-neural-network-enhanced distribution of relaxation times. *Electrochim. Acta* **2023**, *439*, 141499.
- (33) Bonomo, M.; Segura Zarate, A.; Fagiolari, L.; Damin, A.; Galliano, S.; Gerbaldi, C.; Bella, F.; Barolo, C. Unreported resistance in charge transport limits the photoconversion efficiency of aqueous dye-sensitized solar cells: an electrochemical impedance spectroscopy study. *Mater. Today Sustain.* **2023**, *21*, 100271.
- (34) Paraskevaidi, M.; Ashton, K. M.; Stringfellow, H. F.; Wood, N. J.; Keating, P. J.; Rowbottom, A. W.; Martin-Hirsch, P. L.; Martin, F. L. Raman spectroscopic techniques to detect ovarian cancer biomarkers in blood plasma. *Talanta* **2018**, *189*, 281–288.
- (35) Weiland, F.; Fritz, K.; Oehler, M. K.; Hoffmann, P. Methods for Identification of CA125 from Ovarian Cancer Ascites by High Resolution Mass Spectrometry. *Int. J. Mol. Sci.* **2012**, *13*, 9942–9958.
- (36) Gazze, A.; Ademefun, R.; Conlan, R. S.; Ademefun, R.; Teixeira, S. R.; Teixeira, S. R. Electrochemical impedance spectroscopy enabled CA125 detection; toward early ovarian cancer diagnosis using graphene biosensors. *J. Interdiscip. Nanomed.* **2018**, *3*, 82–88.
- (37) Shallan, A. I.; Abdel-Hakim, A.; Hammad, M. A.; Abou El-Alamin, M. M. Spectrofluorimetric determination of selected genotoxic impurities in pharmaceutical raw materials and final products. *Sci. Rep.* **2022**, *12* (1), 15319.
- (38) Hassan, H. M.; Alsohaimi, I. H.; El-Sayed, M. Y.; Ali, I. I.; El-Didamony, A. M.; Altaleb, H. A.; Alshammari, M. S. Selective Spectrofluorimetric Approach for the Assessment of Two Antipsychotic Drugs through Derivatization with O-Phthalaldehyde. *Pharmaceuticals* **2022**, *15* (10), 1174.
- (39) Croce, A. C.; Ferrigno, A.; Berardo, C.; Bottiroli, G.; Vairetti, M.; Di Pasqua, L. G. Spectrofluorometric Analysis of Autofluorescing Components of Crude Serum from a Rat Liver Model of Ischemia and Reperfusion. *Molecules* **2020**, *25* (6), 1327.
- (40) Salem, H.; A Abo Elsoud, F.; Magdy, A.; Heshmat, D.; Elkady, A.; Wissa, K.; Hassan, K.; Abdelrady, R. Spectroscopic Methods for Analysis of Nano Drug Distribution System. *Pharm. Anal. Acta* **2020**, *11*, 619.
- (41) Magno, L. N.; Bezerra, F. C.; Freire, L. E. S.; Guerra, R. A.; Bakuzis, A. F.; Goncalves, P. J. Use of Spectroscopic Techniques for Evaluating the Coupling of Porphyrins on Biocompatible Nanoparticles. A Potential System for Photodynamics, Theranostics, and Nanodrug Delivery Applications. *J. Phys. Chem. A* **2017**, *121* (9), 1924–1931.
- (42) Ratajczak, K.; Grel, H.; Olejnik, P.; Jakiela, S.; Stobiecka, M. Current progress, strategy, and prospects of PD-1/PDL-1 immune checkpoint biosensing platforms for cancer diagnostics, therapy monitoring, and drug screening. *Biosens. Bioelectron.* **2023**, *240*, 115644.
- (43) Stobiecka, M.; Ratajczak, K.; Jakiela, S. Toward early cancer detection: Focus on biosensing systems and biosensors for an anti-apoptotic protein survivin and survivin mRNA. *Biosens. Bioelectron.* **2019**, *137*, 58–71.
- (44) Dong, T.; Zhu, W.; Yang, Z.; Matos Pires, N. M.; Lin, Q.; Jing, W.; Zhao, L.; Wei, X.; Jiang, Z. Advances in heart failure monitoring: Biosensors targeting molecular markers in peripheral bio-fluids. *Biosens. Bioelectron.* **2024**, *255*, 116090.
- (45) Farzin, L.; Shamsipur, M.; Samandari, L.; Sheibani, S.; Sheibania, S. HIV biosensors for early diagnosis of infection: The intertwine of nanotechnology with sensing strategies. *Talanta* **2020**, *206*, 120201.
- (46) Stern, O.; Volmer, M. Über die abklingzeit der fluoreszenz. *Z. Phys.* **1919**, *20*, 183–188.
- (47) ICH. *International Conference on Harmonisation of Technical Requirements for Registration of Pharmaceuticals for Human Use, (ICH) Q2 (R1) Validation of Analytical Procedures: Text and Methodology*, 2005, Vol. 1; pp1–15.
- (48) Abou-Omar, M. N.; Attia, M. S.; Afify, H. G.; Amin, M. A.; Boukherroub, R.; Mohamed, E. H. Novel optical biosensor based on a nano-gold coated by Schiff base doped in sol/gel matrix for sensitive screening of oncomarker CA-125. *ACS Omega* **2021**, *6*, 20812–20821.
- (49) AlGhamdi, H. A.; AlZahrani, Y. M.; Alharthi, S.; Mohy-Eldin, M. S.; Mohamed, E. H.; Mahmoud, S. A.; Attia, M. S. Novel sensor for the determination of CA 15-3 in serum of breast cancer patients based on Fe–gallic acid complex doped in modified cellulose polymer thin films. *RSC Adv.* **2023**, *13* (31), 21769–21780.

- (50) Attia, M. S.; Youssef, A. O.; Khan, Z. A.; Abou-Omar, M. N. Alpha fetoprotein assessment by using a nano optical sensor thin film binuclear Pt-2-aminobenzimidazole-Bipyridine for early diagnosis of liver cancer. *Talanta* **2018**, *186*, 36–43.
- (51) Attia, M. S.; Al-Radadi, N. S. Progress of pancreatitis disease biomarker alpha amylase enzyme by new nano optical sensor. *Biosens. Bioelect.* **2016**, *86*, 413–419.
- (52) Attia, M. S.; Khalil, M. H.; Abdel-Mottaleb, M. S. A.; Lukyanova, M. B.; Alekseenko, Yu. A.; Lukyanov, B. Effect of complexation with lanthanide metal ions on the photochromism of (1, 3, 3-trimethyl-5'-hydroxy-6'-formyl-indoline-spiro2, 2'-[2h] chromene) in different media. *Int. J. Photoenergy* **2006**, *2006*, 1–9.
- (53) Attia, M. S.; Youssef, A. O.; Essawy, A. A. A novel method for tyrosine assessment in vitro by using fluorescence enhancement of the ion-pair tyrosine-neutral red dye photo probe. *Anal. Methods* **2012**, *4*, 2323–2328.
- (54) Attia, M. S.; Ali, K.; El-Kemary, M.; Darwish, W. M. Phthalocyanine-doped polystyrene fluorescent nanocomposite as a highly selective biosensor for quantitative determination of cancer antigen 125. *Talanta* **2019**, *201*, 185–193.
- (55) Attia, M. S.; Mahmoud, W. H.; Youssef, A. O.; Mostafa, M. S. Cilostazol determination by the enhancement of the green emission of Tb³⁺ optical sensor. *J. Fluoresc.* **2011**, *21*, 2229–2235.
- (56) Attia, M. S.; Ramsis, M. N.; Khalil, L. H.; Hashem, S. G. Spectrofluorimetric assessment of chlorzoxazone and Ibuprofen in pharmaceutical formulations by using Eu-tetracycline HCl optical sensor doped in sol-gel matrix. *J. Fluoresc.* **2012**, *22*, 779–788.
- (57) Attia, M. S.; Mahmoud, W. H.; Ramsis, M. N.; Khalil, L. H.; Othman, A. M.; Hashem, S. G.; Mostafa, M. S. Spectrofluorimetric assessment of doxycycline hydrochloride in pharmaceutical tablets and serum sample based on the enhancement of the luminescence intensity of the optical sensor Sm³⁺ ion. *J. Fluoresc.* **2011**, *21*, 1739–1748.
- (58) Attia, M. S.; Othman, A. M.; Elraghi, E.; Aboul-Enein, H. Y. Spectrofluorimetric assessment of metoclopramide hydrochloride using terbium doped in PMMA matrix optical sensor. *J. Fluoresc.* **2011**, *21*, 739–745.
- (59) Elabd, A. A.; Attia, M. S. Spectrofluorimetric assessment of UO₂²⁺ by the quenching of the fluorescence intensity of Clopidogrel embedded in PMMA matrix. *J. Lumin.* **2016**, *169*, 313–318.
- (60) Attia, M. S.; Bakir, E.; Abdel-Aziz, A. A.; Abdel-Mottaleb, M. S. A. Determination of melamine in different milk batches using a novel chemosensor based on the luminescence quenching of Ru (II) carbonyl complex. *Talanta* **2011**, *84*, 27–33.
- (61) Attia, M. S.; Elsaadany, S. A.; Ahmed, K. A.; El-Molla, M. M.; Abdel-Mottaleb, M. S. A. Inkjet Printable Luminescent Eu³⁺-TiO₂ Doped in Sol Gel Matrix for Paper Tagging. *J. Fluoresc.* **2015**, *25*, 119–125.
- (62) Hashem, S. G.; Elsaady, M. M.; Afify, H. G.; Omer, W. E.; Youssef, A. O.; El-Kemary, M.; Attia, M. S. Determination of uric acid in serum using an optical sensor based on binuclear Pd (II) 2-pyrazinecarboxamide-bipyridine doped in a sol gel matrix. *Talanta* **2019**, *199*, 89–96.
- (63) Abdel-Mottaleb, M. S. A.; Saif, M.; Attia, M. S.; Abo-Aly, M. M.; Mobarez, S. N. Lanthanide complexes of spiropyran photoswitch and sensor: spectroscopic investigations and computational modelling. *Photochem. Photobiol. Sci.* **2018**, *17*, 221–230.
- (64) Omer, W. E.; El-Kemary, M. A.; Elsaady, M. M.; Abou-Omar, M. N.; Youssef, A. O.; Sayqal, A. A.; Gouda, A. A.; Attia, M. S. Highly efficient gold nano-flower optical biosensor doped in a sol-gel/PEG matrix for the determination of a calcitonin biomarker in different serum samples. *ACS Omega* **2020**, *5*, 5629–5637.
- (65) Abdullah, L. A.; Attia, M.; Abdel-Mottaleb, M. S. Nalbuphine HCl Assessment by the Quenching of the Emission of Tb –4'Carboxybenzo-18crown-6-Ether Optical Sensor. *Egy. J. Chem.* **2019**, *62*, 247–255.
- (66) Gasparotto, G.; Costa, J. P.; Costa, P. I.; Zaghete, M. A.; Mazon, T. Electrochemical immunosensor based on ZnO nanorodsAu nanoparticles nanohybrids for ovarian cancer antigen CA-125 detection. *Mater. Sci. Eng., C* **2017**, *76*, 1240–1247.
- (67) Torati, S. R.; Kasturi, K. C.; Lim, B.; Kim, C. Hierarchical gold nanostructures modified electrode for electrochemical detection of cancer antigen CA125. *Sens. Actuators, B* **2017**, *243*, 64–71.
- (68) Johari-Ahar, M.; Rashidi, M. R.; Barar, J.; Aghaie, M.; Mohammadnejad, D.; Ramazani, A.; Karami, P.; Coukos, G.; Omid, Y. An ultra-sensitive impedimetric immunosensor for detection of the serum oncomarker CA-125 in ovarian cancer patients. *Nanoscale* **2015**, *7*, 3768–3779.
- (69) Raghav, R.; Srivastava, S. Core-shell gold-silver nanoparticles based impedimetric immunosensor for cancer antigen CA125. *Sens. Actuators, B* **2015**, *220*, 557–564.
- (70) Xie, L.; Cao, Y.; Hu, F.; Li, T.; Wang, Q.; Gan, N. Microfluidic chip electrophoresis for simultaneous fluorometric aptasensing of alpha-fetoprotein, carbohydrate antigen 125 and carcinoembryonic antigen by applying a catalytic hairpin assembly. *Microchim. Acta* **2019**, *186*, 547.
- (71) Hamd-Ghadareh, S.; Salimi, A.; Parsa, S.; Fathi, F. Simultaneous biosensing of CA125 and CA15–3 tumor markers and imaging of OVCAR-3 and MCF-7 cells lines via bi-color FRET phenomenon using dual blue-green luminescent carbon dots with single excitation wavelength. *Int. J. Biol. Macromol.* **2018**, *118*, 617–628.
- (72) Attia, M. S.; Ali, K.; El-Kemary, M.; Darwish, W. M. Phthalocyanine-doped polystyrene fluorescent nanocomposite as a highly selective biosensor for quantitative determination of cancer antigen 125. *Talanta* **2019**, *201*, 185–193.